

The phase structure of QCD for heavy quarks

Christian S. Fischer,¹ Jan Luecker,^{2,3} and Jan M. Pawłowski³

¹*Institut für Theoretische Physik, Justus-Liebig-Universität Gießen,
Heinrich-Buff-Ring 16, D-35392 Gießen, Germany.*

²*Institut für Theoretische Physik, Goethe-Universität Frankfurt,
Max-von-Laue-straße 1, D-60438 Frankfurt/Main, Germany*

³*Institut für Theoretische Physik, Universität Heidelberg, Philosophenweg 16, 69120 Heidelberg, Germany*

(Dated: October 1, 2014)

We investigate the nature of the deconfinement and Roberge-Weiss transition in the heavy quark regime for finite real and imaginary chemical potential within the functional approach to continuum QCD. We extract the critical phase boundary between the first order and cross-over regions, and also explore tricritical scaling. Our results confirm previous ones from finite volume lattice studies.

I. INTRODUCTION

The phase structure of QCD at finite temperature and density is a very active research topic explored experimentally in heavy ion collisions at RHIC, the LHC and the future NICA and FAIR facilities. One of the most interesting problems concerns the possible appearance of a critical end point at finite chemical potential μ , connecting the chiral and deconfinement crossover region at small μ with the first order transition at large chemical potential. In this region of the phase diagram, lattice QCD is severely hampered by the fermion sign problem preventing continuum extrapolated studies with contemporary resources, see e.g. [1, 2] for reviews. First principle continuum methods such as the approach via Dyson-Schwinger and functional renormalization group equations avoid this problem at the expense of truncations, that need to be controlled. At finite real and imaginary chemical potential such control is possible in the heavy quark region, which provides an interesting playground with interesting physical phenomena well worth studying in their own right.

At zero chemical potential and infinite quark mass, i.e. in the quenched approximation of QCD, the Polyakov loop expectation value exhibits a discontinuity which is associated with a first order deconfinement transition. However, due to the center-symmetry breaking effect of dynamical quarks, this transition is known to be a crossover for physical quark masses [3–5]. It follows that a critical quark mass exists, where the first order phase transition changes into a crossover. This situation is usually represented in the upper right corner of the Columbia plot, see Fig. 1. This regime of QCD has been studied in lattice simulations, where due to the large quark masses the sign problem becomes treatable, and hence the extension to finite chemical potential is also feasible [7–10]. Then the critical line extends to a critical surface, which has been studied for real and imaginary chemical potential [9]. QCD at (unphysical) imaginary chemical potential does not suffer from a sign problem even at small quark masses, as γ_5 hermiticity is restored. Such an extension is of high interest as it allows to study QCD in a fugacity expansion. Moreover, the study of the analytic

structure of the critical surface at large quark masses may give hints at how to extend the critical surface at small quark masses from imaginary chemical potential to real chemical potential.

In this work we apply the continuum Dyson-Schwinger approach to QCD in the heavy quark limit. Our approximation scheme explicitly takes into account the back-reaction of the quarks onto the Yang-Mills sector thus rendering a systematic exploration of the physics of the Columbia plot possible [11, 12]. We are therefore able to calculate the Polyakov-loop potential explicitly using a DSE for the background gauge field [13, 14]. For applications within functional approaches see [15–19]. This approach allows us to study the physics of the deconfinement transition directly without the need for any *ansätze* for the potential as has been used in model studies, e.g. [20, 21]. In this framework we explore the heavy quark regime and determine the critical surface of the deconfinement transition. In our continuum approach we find tricritical scaling in agreement with the finite volume lattice studies.

This letter is organized as follows: In the next section we present some technical details related to our approach. We then discuss our results for zero, real and imaginary chemical potential in section III before we conclude in section V.

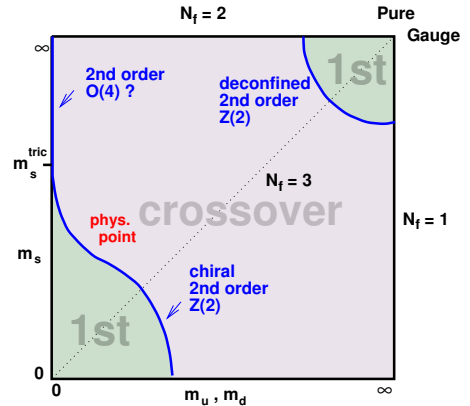


FIG. 1. The Columbia plot, taken from [6].

$$\frac{\delta(\Gamma - S)}{\delta A_0} = \frac{1}{2} \left(\text{ghost self-energy} - \text{gluon self-energy} - \text{ghost-gluon loop} - \frac{1}{6} \left(\text{two-loop ghost-gluon loop} + \text{two-loop ghost-gluon-ghost loop} \right) \right)$$

FIG. 2. The DSE for background field \bar{A} .

II. SET-UP

A. Polyakov-loop potential

In the heavy quark limit of QCD, confinement is associated to center symmetry. The expectation value of the Polyakov loop, $\langle L[A_0] \rangle$, serves as an order parameter for center symmetry. It is linked to the free energy of a quark-anti-quark pair at infinite distance. $\langle L[A_0] \rangle$ is the minimum of the order parameter potential $\Omega(L)$. This potential is often used as input in enhanced model studies. An alternative order parameter is $L[\bar{A}_0]$, with background field \bar{A}_0 , that satisfies the quantum equation of motion [22, 23]. The two are related by

$$L[\bar{A}_0] \geq \langle L[A_0] \rangle \quad \text{and} \quad \langle L[A_0] \rangle = 0 \rightarrow L[\bar{A}_0] = 0, \quad (1)$$

where

$$L[A_0] = \frac{1}{N_c} \text{Tr}_c \mathcal{P} \left[e^{i g \int_0^\beta dx_0 A_0(x_0, \vec{x})} \right], \quad (2)$$

is the Polyakov loop for a gauge field A , \mathcal{P} stands for path ordering and $\beta = 1/T$ is the inverse temperature. The two relations in (1) mark $L[\bar{A}_0]$ as an order parameter.

In the theory with background field, the DSE for this field has been derived in [13], see Fig. 2. This DSE describes the derivative of the background-field potential $V(\bar{A}_0) = \Omega(L)$. From the minimum of the potential, we get the order parameters \bar{A}_0 and $L[\bar{A}_0]$.

Constant background fields can always be rotated in the Cartan sub-algebra of the $SU(3)$ color group. In the fundamental representation the background field is then decomposed to

$$\bar{A}_0 = \frac{2\pi T}{g} \left(\varphi_3 \frac{\lambda_3}{2} + \varphi_8 \frac{\lambda_8}{2} \right), \quad (3)$$

with Gell-Mann matrices λ_a . The Polyakov loop $L[\bar{A}_0]$ reads

$$L[\bar{A}_0] = \frac{1}{3} \left[e^{-i \frac{2\pi\varphi_8}{\sqrt{3}}} + 2e^{-i \frac{\pi\varphi_8}{\sqrt{3}}} \cos(\pi\varphi_3) \right], \quad (4)$$

a complex function, which is real for $\varphi_8 = 0$.

In [14] the background-field DSE has been used to study the Polyakov loop potential for QCD at finite density, and we will build upon this work. It has been argued in [13] that the two-loop terms in Fig. 2 can be neglected in an optimized regularization scheme and for temperatures not too far away from the critical temperature. In

$$\text{quark DSE: } \text{bare quark} \xrightarrow{-1} = \text{dressed quark} \xrightarrow{-1} + \text{quark-gluon loop} \xrightarrow{-1}$$

$$\text{gluon DSE: } \text{bare gluon} \xrightarrow{-1} = \text{dressed gluon} \xrightarrow{-1} + N_f \text{gluon loop} \xrightarrow{-1}$$

FIG. 3. The DSEs for quark and gluon propagators.

the present work we are interested in the physics close to the critical surface and hence the two-loop terms can be safely dropped. Then the Polyakov-loop potential is completely determined by the quark, gluon and ghost propagators.

B. Propagators

It is left to determine gluon, ghost and quark propagators. The computation is based on the quenched ghost and gluon propagators at finite temperature obtained within the functional renormalisation group approach in [24]. We use the quenched ghost in the following: at vanishing density both thermal and quantum fluctuations of the matter sector have a negligible impact on the ghost propagator, it keeps its quenched form. As density fluctuations are transmitted via the matter sector, this behaviour can be extended to finite density. In contrast, it is mandatory for quantitative precision to unquench the gluon. To this end, we solve quark and gluon DSEs in a truncation that has been developed in [11, 12]; the truncated DSEs are shown in Fig. 3.

The bare quark propagator is given by

$$S_0^{-1}(p) = i(\omega_n + i\mu)\gamma_4 + i\vec{p}\vec{\gamma} + Z_m m, \quad (5)$$

where $m(\zeta)$ is the renormalized bare quark mass at renormalization point ζ and $Z_m(\zeta)$ its renormalization factor. For the calculation we use $\zeta = 80$ GeV. The quark mass is the main parameter, which we will tune in order to find its critical value m_c , where the phase transition is of second order.

For the quark-gluon vertex we choose the same ansatz that has been shown to give excellent results in comparison with lattice QCD at small quark masses in Ref. [11, 12]. The only change is related to the infrared strength of the quark-gluon interaction controlled by a parameter d_1 . In [25], the DSE for the quark-gluon vertex has been solved at zero temperature in a truncation that allowed to extract the quark mass dependence of the vertex. Guided by these results, we infer a reduction of the vertex strength from $d_1 \approx 8$ GeV² to the value $d_1 = 0.5$ GeV² used in this study.

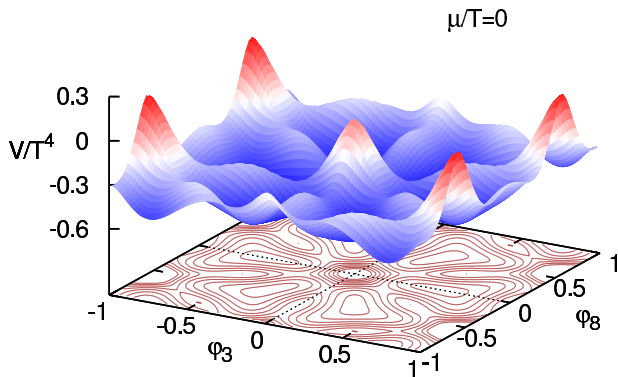


FIG. 4. Polyakov-loop potential at $\mu = 0$ in the approximately center symmetric phase.

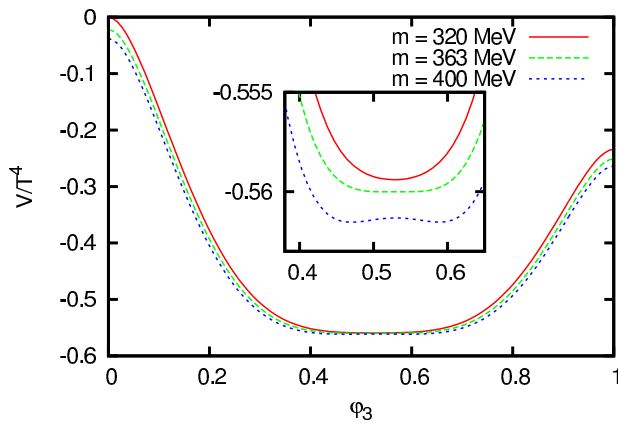


FIG. 5. The potential at T_c for quark masses below, at and above $m_c = 363$ MeV for $N_f = 1$ and $\mu = 0$. The potentials have been shifted arbitrarily for better visibility.

III. DETERMINATION OF CRITICAL QUARK MASSES

A. Zero density

We show the Polyakov-loop potential at $\mu = 0$ in Fig. 4 as a function of φ_3 and φ_8 for $T = 250$ MeV and $m = 320$ MeV in the approximately center-symmetric phase. Here, the potential has six degenerate minima located close to $(\varphi_3, \varphi_8) = (\pm 2/3, 0)$ and $(\varphi_3, \varphi_8) = (\pm 1/3, \pm 1/\sqrt{3})$ rendering $L[\bar{A}_0] \approx 0$. Consider now the minimum at $(\varphi_3, \varphi_8) = (2/3, 0)$. At the critical temperature T_c a first order phase transition can clearly be distinguished from a crossover by the emergence of a two-minima structure of the potential as a function of φ_3 around T_c . At the critical quark mass m_c the two-minima structure changes to a single minimum. For smaller masses, $m < m_c$, we have a crossover. The related critical temperature in this region is not unique and we extract it with the inflection point $\max(\partial_T L[\bar{A}_0])$. The three different regions, first order regime, critical point, crossover regime, are visualized in Fig. 5, where we show the po-

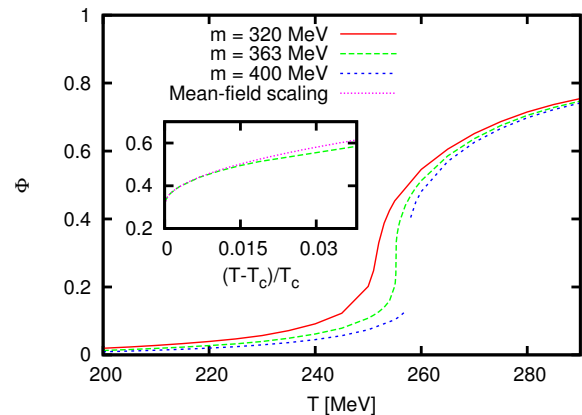


FIG. 6. The Polyakov loop $L[A_0]$ for the same quark masses as in Fig. 5 for $N_f = 1$ and $\mu = 0$.

N_f	m_c [MeV]	m_c/T_c
1	363	1.422
2	461	1.827
3	509	2.038

TABLE I. Critical current quark mass $m_c(\zeta = 80 \text{ GeV})$.

tential at the critical temperature for three quark masses, which are below, at and above the critical quark mass. For $m < m_c$ we find only one minimum away from the confining value $\varphi_3 = \frac{2}{3}$. At $m = m_c$ the potential is flat. For $m > m_c$ we have two degenerate minima. The structure of the potential reflects itself in the behaviour of the order parameter, the Polyakov loop, which is shown in Fig. 6 as a function of T for the same quark masses as used for the potential in Fig. 5. One can clearly distinguish the crossover for $m < m_c$ from the very sharp first order transition at $m > m_c$. At $m = m_c$ we have a second order phase transition. The critical exponent β is derived from the order parameter with $L[\bar{A}_0] \sim |T - T_c|^\beta$ in the vicinity of T_c . In our approximation we extract $\beta = 1/2$, the mean-field critical exponent. This is to be expected as the current approximation to the Polyakov loop potential neglects the backreaction relevant for criticality, see [13, 23].

In Tab. I we list the resulting critical quark masses for $N_f \in \{1, 2, 3\}$. Note that the current quark mass depends on the renormalization point and scheme. Therefore a direct comparison of our results for m_c to the lattice results is difficult and will be postponed. We came back to this point in section IV.

B. Real chemical potential

For real chemical potential and non-vanishing background fields the quark contribution to the Polyakov-loop potential $V(\bar{A}_0)$ is complex for general (φ_3, φ_8) . However, a modified real effective potential can be con-

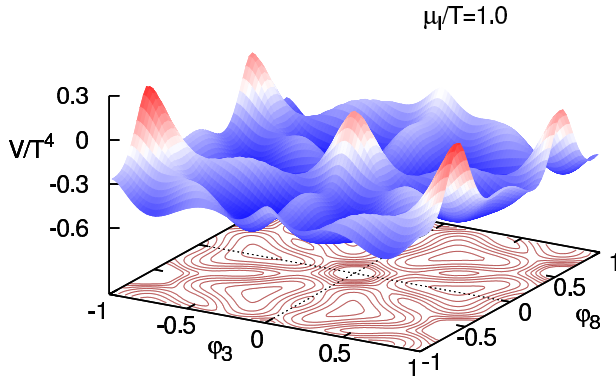


FIG. 7. Polyakov-loop potential at $\mu_I/T = 1.0$, $T = 250$ MeV, $m = 320$ MeV.

structured that agrees with $V(\bar{A}_0)$ on the equations of motion, [26]. This procedure is consistent with taking $\varphi_8 = 0$, leading to a real potential. For this choice the same procedure to find m_c as in the $\mu = 0$ case can be used. The chemical potential affects the Polyakov loop potential dominantly through the quark loop in Fig. 2, but also through the back-reaction of the quarks onto the gluon, see Fig. 3. We show the resulting critical quark masses in Sec. IV.

C. Imaginary chemical potential

At imaginary chemical potential $\mu_I = \mu/i = 2\pi T\theta$ QCD features the Roberge-Weiss symmetry [27], which states that QCD is periodic in θ with periodicity $1/N_c$ defined by the gauge group. Above the Roberge-Weiss critical point, QCD exhibits first order phase transitions with the Polyakov loop proportional to different center elements across the transitions. In the functional approach, the physics of these transitions has been studied in Ref. [15]. We built upon this framework here and repeat the basic ideas in the following.

In the presence of an imaginary chemical potential, the quark Matsubara modes are shifted by μ_I as well as A_0 , the full gauge field.

$$\omega_n \rightarrow \omega_n + g A_0 + 2\pi T\theta. \quad (6)$$

For an Abelian gauge field A_0 , the imaginary chemical potential $\mu_I = 2\pi T\theta$ could be reabsorbed in the gauge field by a shift leading to $g\tilde{A}_0 = gA_0 + 2\pi T\theta$. This is a constant shift of the gauge field and does not change the gauge action. For an $SU(N)$ -gauge field this is not possible as it has no $U(1)$ -component. However, we can use

$$\tilde{\varphi}_3 = \varphi_3 + 3\theta, \quad \tilde{\varphi}_8 = \varphi_8 + \sqrt{3}\theta, \quad (7)$$

and \tilde{A}_0 is the field with φ_i replaced by $\tilde{\varphi}_i$. With this shift, we can write Eq. (6) as

$$\omega_n \delta_{ij} + g A_{0,ij} + 2\pi T\theta \delta_{ij} \rightarrow \omega_n \delta_{ij} + g \tilde{A}_{0,ij} + 3(2\pi T)\theta \delta_{i1}. \quad (8)$$

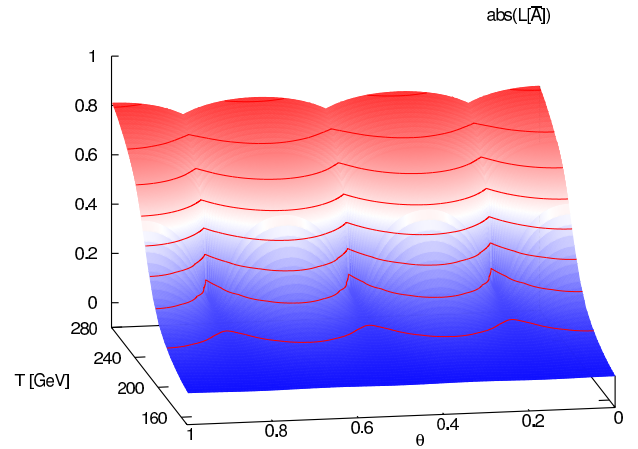


FIG. 8. Absolute value of the Polyakov loop at $m = 200$ MeV for $N_f = 2$.

In this form the Roberge-Weiss symmetry is manifest: a shift in the imaginary potential by $\theta \rightarrow \theta + \theta_z$ with $\theta_z = k/3$, $k \in \mathbb{Z}$ can be absorbed by a shift in the Matsubara sum and a center transformation in the gauge field. As a center transformation is reflected by a rotation of the Polyakov loop in the complex plane, the Polyakov loop must be defined complex at imaginary chemical potential.

The minima of the Polyakov loop potential are therefore not at $\varphi_8 = 0$, as the latter implies a vanishing $\arg(L[\tilde{A}])$. The potential for a non-vanishing θ as a function of φ_3, φ_8 is shown in Fig. 7. The minimum is shifted away from $\varphi_8 = 0$, implying a complex Polyakov loop. In contrast to the situation at real chemical potential, the potential stays real at imaginary chemical potential for all φ_8 .

To demonstrate the effect of the imaginary chemical potential on the Polyakov loop, we show the absolute value and the argument of the Polyakov loop, respectively in Figs. 8,9 for $m = 200$ MeV and $N_f = 2$. The Roberge-Weiss symmetry is apparent. Above a critical temperature of about 240 MeV, $\arg(L[\tilde{A}])$ shows a jump at $\mu_I/T = \frac{\pi}{3}(2k+1)$, $k \in \mathbb{Z}$. This is the Roberge-Weiss phase transition, where the phase of the Polyakov loop expectation value jumps. At asymptotically large temperatures it jumps from one center element to the next. At the value of the quark mass used for Fig. 8, the Polyakov loop shows a crossover at all values of θ up to the critical value $\theta_c = 1/6$. For a larger value of the quark mass, a critical end-point appears for some θ at which the transition turns first order. At the critical quark masses given in Tab. I this end-point is at $\theta = 0$.

IV. RESULTS FOR ALL CHEMICAL POTENTIALS

The main result of this work is given in Fig. 10, where we show m_c/T as a function of μ^2/T^2 for $N_f \in \{1, 2, 3\}$ starting at the critical surface where $\mu/T = i\pi/3$. We

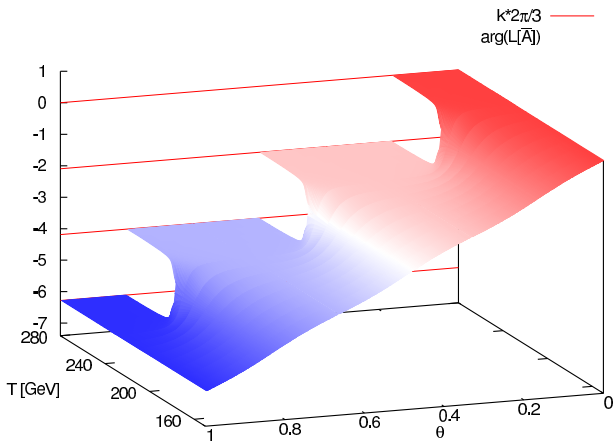


FIG. 9. Angle of the Polyakov loop at $m = 200$ MeV for $N_f = 2$.

N_f	K	m_{tric}/T
1	0.98	0.406
2	0.94	0.852
3	0.90	1.109

TABLE II. Fit results for Eq. (9).

compare our results to tricritical scaling, given by

$$\frac{m_c}{T} = \frac{m_{tric}}{T} + K \left[\left(\frac{\pi}{3} \right)^2 + \left(\frac{\mu}{T} \right)^2 \right]^{2/5}, \quad (9)$$

where m_{tric} is the quark mass on the tricritical surface $\mu_I/T = \pi/3$ and K is a parameter that we determine by fitting. In [9] it has been found that lattice results for m_c/T are well described by tricritical scaling, Eq. (9), up to large chemical potentials. As Fig. 10 shows, we find slight deviations from the scaling behaviour with our critical quark masses slightly above the scaling curve. This has also been observed on the lattice [9]. Thus we find nice qualitative agreement with the lattice results at all chemical potentials.

The results for the parameters K and m_{tric} for the tricritical scaling can be found in Tab. II. When we compare to those values given in [9] we find that our critical quark masses are consistently smaller. This is certainly due to the different definition of the quark mass, which depends strongly on the renormalisation point and scheme and potentially also on the lattice volume. In order to make quantitative statements one would have to compare appropriate quantities as for example the corresponding quark propagators, see e.g. [28] for such a comparison. Since these are not yet available from the lattice, we postpone this to future work.

In order to make the connection to the Columbia plot, Fig. 1, we show in Fig. 11 a three-dimensional version of the Columbia plot, with $(\mu/T)^2$ as a third axis. The first order area starts at the critical surface with $(\mu/T)^2 =$

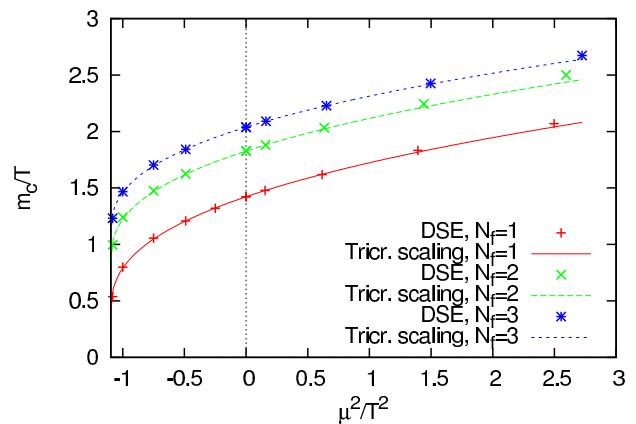


FIG. 10. The critical quark mass as a function of $(\mu/T)^2$.

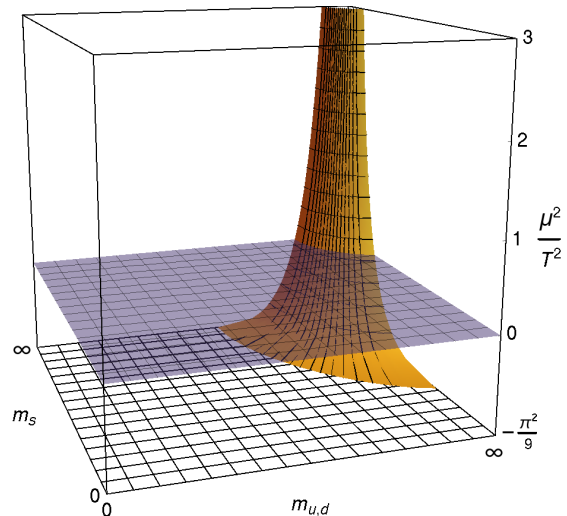


FIG. 11. The three-dimensional Columbia plot. The quark masses are scaled according to $f : [0, \infty] \rightarrow [0, 1]$, $f(m) = 1 - e^{-m/T}$.

$-(\pi/3)^2$ and shrinks for growing μ^2 . For Fig. 11 we also obtained the critical quark masses for $N_f = 2 + 1$ case with $m_l \neq m_s$ at $(\mu/T)^2 \in \{-1.04^2, 0, 1.4^2\}$ and continue these values by a fit for $m_{s,c}(m_{l,c})$ and tricritical scaling for the μ -dependence.

V. CONCLUSIONS

We have used an established truncation for the quark and gluon DSEs in order to access the Polyakov-loop potential of full QCD at real and imaginary chemical potential. For large quark masses, we find an area where the phase transition is of first order, bounded by a line of second order phase transitions. This is the expected scenario from the Columbia plot. As a function of μ^2 the critical quark masses are in qualitative agreement with lattice results. The level of quantitative agreement is hard to access, since the definition of the quark mass is different.

Given the quality of our description of the physics of confinement, it is a logical extension to also investigate the physics of the chiral sector, i.e. the lower left corner of the Columbia plot, Fig. 1. There, the important physics is not the Polyakov-loop potential but the Goldstone bosons of chiral symmetry. Since those are currently not included in our truncation, we can not expect a valid description of this area so far. However, it is possible to include the back-reaction of the Goldstone bosons onto the quarks in the DSE language, see e.g. [29]. An extension of this work will therefore be able to describe the critical physics of confinement and chiral symmetry breaking at all quark masses and chemical potentials.

ACKNOWLEDGEMENTS

We would like to thank Leonard Fister for discussions and work on related projects and Bernd-Jochen Schaefer for a critical reading of the manuscript. This work is supported by the Helmholtz Alliance HA216/EMMI, by ERC-AdG-290623, by the Helmholtz International Center for FAIR within the LOEWE program of the State of Hesse and by the BMBF grant 05P12VHCTG.

-
- [1] O. Philipsen, arXiv:1009.4089 [hep-lat].
 - [2] G. Aarts, PoS **LATTICE2012**, 017 (2012), arXiv:1302.3028 [hep-lat].
 - [3] Y. Aoki, G. Endrodi, Z. Fodor, S. Katz, and K. Szabo, Nature **443**, 675 (2006), arXiv:hep-lat/0611014 [hep-lat].
 - [4] A. Bazavov, T. Bhattacharya, M. Cheng, C. Detar, H. Ding, *et al.*, Phys.Rev. **D85**, 054503 (2012), arXiv:1111.1710 [hep-lat].
 - [5] T. Bhattacharya, M. I. Buchoff, N. H. Christ, H. T. Ding, R. Gupta, *et al.*, Phys.Rev.Lett. **113**, 082001 (2014), arXiv:1402.5175 [hep-lat].
 - [6] P. de Forcrand and O. Philipsen, Phys.Rev.Lett. **105**, 152001 (2010), arXiv:1004.3144 [hep-lat].
 - [7] C. Alexandrou, A. Borici, A. Feo, P. de Forcrand, A. Galli, *et al.*, Phys.Rev. **D60**, 034504 (1999), arXiv:hep-lat/9811028 [hep-lat].
 - [8] H. Saito *et al.* (WHOT-QCD Collaboration), Phys.Rev. **D84**, 054502 (2011), arXiv:1106.0974 [hep-lat].
 - [9] M. Fromm, J. Langelage, S. Lottini, and O. Philipsen, JHEP **1201**, 042 (2012), arXiv:1111.4953 [hep-lat].
 - [10] H. Saito, S. Ejiri, S. Aoki, K. Kanaya, Y. Nakagawa, *et al.*, (2013), arXiv:1309.2445 [hep-lat].
 - [11] C. S. Fischer and J. Luecker, Phys.Lett. **B718**, 1036 (2013), arXiv:1206.5191 [hep-ph].
 - [12] C. S. Fischer, J. Luecker, and C. A. Welzbacher, Phys.Rev. **D90**, 034022 (2014), arXiv:1405.4762 [hep-ph].
 - [13] L. Fister and J. M. Pawłowski, Phys.Rev. **D88**, 045010 (2013), arXiv:1301.4163 [hep-ph].
 - [14] C. S. Fischer, L. Fister, J. Luecker, and J. M. Pawłowski, Phys.Lett. **B732**, 273 (2014), arXiv:1306.6022 [hep-ph].
 - [15] J. Braun, L. M. Haas, F. Marhauser, and J. M. Pawłowski, Phys.Rev.Lett. **106**, 022002 (2011), arXiv:0908.0008 [hep-ph].
 - [16] R. Stiele, L. M. Haas, J. Braun, J. M. Pawłowski, and J. Schaffner-Bielich, PoS **ConfinementX**, 215 (2012), arXiv:1303.3742 [hep-ph].
 - [17] T. K. Herbst, M. Mitter, J. M. Pawłowski, B.-J. Schaefer, and R. Stiele, PoS **QCD-TNT-III**, 030 (2013), arXiv:1401.1735 [hep-ph].
 - [18] K. Fukushima and K. Kashiwa, Phys.Lett. **B723**, 360 (2013), arXiv:1206.0685 [hep-ph].
 - [19] U. Reinosa, J. Serreau, M. Tissier, and N. Wschebor, (2014), arXiv:1407.6469 [hep-ph].
 - [20] K. Kashiwa, R. D. Pisarski, and V. V. Skokov, Phys.Rev. **D85**, 114029 (2012), arXiv:1205.0545 [hep-ph].
 - [21] P. M. Lo, B. Friman, and K. Redlich, (2014), arXiv:1406.4050 [hep-ph].
 - [22] J. Braun, H. Gies, and J. M. Pawłowski, Phys.Lett. **B684**, 262 (2010), arXiv:0708.2413 [hep-th].
 - [23] F. Marhauser and J. M. Pawłowski, (2008), arXiv:0812.1144 [hep-ph].
 - [24] L. Fister and J. M. Pawłowski, (2011), arXiv:1112.5440 [hep-ph].
 - [25] R. Williams, arXiv:1404.2545 [hep-ph].
 - [26] J. M. Pawłowski, in preparation.
 - [27] A. Roberge and N. Weiss, Nucl.Phys. **B275**, 734 (1986).
 - [28] C. Fischer and M. Pennington, Phys.Rev. **D73**, 034029 (2006), arXiv:hep-ph/0512233 [hep-ph].
 - [29] C. S. Fischer and J. A. Mueller, Phys.Rev. **D84**, 054013 (2011), arXiv:1106.2700 [hep-ph].